American Journal of Applied Sciences

Original Research Paper

$KMnO_4$ Modified Carbon Prepared from Waste of Pineapple Leaf Fiber Production Processing for Removal of Ferric Ion from Aqueous Solution

Sumrit Mopoung and Thaksaphon Bunterm

Department of Chemistry, Faculty of Science, Naresuan University, Phitsanulok, Thailand

Article history
Received: 01-03-2016
Revised: 23-06-2016
Accepted: 24-06-2016

Corresponding Author:
Sumrit Mopoung
Department of Chemistry, Faculty of Science, Naresuan University, Phitsanulok, Thailand
Email: sumritm@nu.ac.th

Abstract: $KMnO_4$ modified carbon materials from waste of pineapple leaf fiber production processing were prepared and characterized. The effects of % weight of $KMnO_4$ (0-5 %wt) and carbonization temperature (500-700°C) were studied by SEM-EDS, XRD, FTIR and BET. The $KMnO_4$ modified waste carbon was used for Fe^{3+} removal from aqueous solutions. The effects of $KMnO_4$ modification, contact time, pH and loading were evaluated. The Langmuir isotherm and Freundlich isotherm were also used for evaluation of Fe^{3+} adsorption by $KMnO_4$ modified waste carbon. The results show that MnO_2 deposited on the surface of $KMnO_4$ modified waste carbon with some heterogeneity. The OH, CO and MnO groups are major functional groups on the surface of $KMnO_4$ modified carbon. The BET surface area and total pore volume of modified waste carbon is increased with increasing weight % of $KMnO_4$ and carbonization temperature, while the average pore size follows an inverse trend. The Fe^{3+} adsorption on modified waste carbon reaches equilibrium within 60 min. The amount of Fe^{3+} adsorbed on the modified waste carbon increases with increasing pH, reaches maximum at pH of about 4.7 and then sharply decreases at pH above 7. Both Langmuir and Freundlich isotherms were fitted for data a Fe^{3+} adsorption on modified waste carbon with 25.25 mg g^{-1} as theoretical maximum adsorption capacity.

Keywords: Carbon, Potassium Permanganate, Pineapple Leaf Fiber Waste, Ferric Ion

Introduction

Pineapple is a food plant, which is grown in many countries. After harvesting, large quantities of pineapple leaves are left behind as waste causing various problems for farmers. This material has been used for pineapple leaf fiber production by mechanical milling process (Kengkhetkit and Amornsakchai, 2012). Milled materials form mechanical milling processing are pineapple leaf fiber and non-fibrous material. The non-fibrous material (or pineapple fiber waste) constitutes waste from this process and has been previously modified with H_3PO_4 (Mopoung *et al*., 2016). The carbon content of pineapple fiber waste is high amounts sufficient (49.03%) to produce charcoal and activated carbon. After carbonization at 500-700°C, the charcoal products of pineapple fiber waste have BET surface area of 48.4335-413.3908 m^2/g (Mopoung *et al*., 2016). Potassium permanganate has the formula $KMnO_4$ and is highly reactive. The reactivity of potassium permanganate depends on pH. It is a strong oxidant at pH lower than 7, but only a mild oxidant in alkaline solutions (Zhang *et al*., 2013b). The surface carbons modified with MnO_4^- are amphoteric and therefore can adsorb both negatively and positively charged contaminants. At pH $<pH_{pzc}$, manganese oxides are positively charged, which leads to attraction of anions such as fluorides. However, in basic solution, manganese oxides become negatively charged and attract cations (Daifullah *et al*., 2007). A composite material with negative charge has also been produced by oxidation with $KMnO_4$ (Arulraj and Rajamathi, 2013). It has been used for as catalysts for oxidation of phenolic compounds at 100°C (Abecassis-Wolfovich *et al*., 2005), cyclization of carbon fiber (Mathur *et al*., 1994), oxidation of hydroxylamine for H_2O_2 production (Song *et al*., 2010)

and oxidation of trichloroethene (Liang *et al*., 2014). The oxidation of carbon based materials by $KMnO_4$ with the aim of removal of natural organic matter has been studied by Zhang *et al*. (2013b). It has been used for water treatment from domestic and industrial sources (Zeid *et al*., 1995). It is also used for drinking water production (Tian *et al*., 2013). It could also improve the surface of active carbons for adsorption of contaminants such as NH_3 (Shan *et al*., 2008), Cd^{2+} (Luo *et al*., 2013), Pb^{2+} (Wang *et al*., 2012), Hg, NO and SO_2 (Ping *et al*., 2012), Cu^{2+} (Baccar *et al*., 2009), Bi^{3+} (Zhang *et al*., 2009) and the removal of *Microcystis Aeruginosa* cell (Waller *et al*., 2014).

In this research we studied the modification of Pineapple Fiber Waste Carbon (PFWC) with $KMnO_4$ and the properties of the resultant material for Fe^{3+} removal from aqueous solution. The effect of $KMnO_4$ concentration was evaluated. The isotherms of Fe adsorption were also evaluated.

Materials and Methods

$KMnO_4$ Modified PFWC Preparation

Pineapple Fiber Waste **(**PFW), which is collected from mechanical milling process for the pineapple leaf fiber production, was used as the precursor material in this study. It consists of 1.15% ash, 49.03% C, 45.54% O, 1.16% Si, 1.15% P, 0.93% K and 0.86% Ca (Mopoung *et al*., 2016). It was cleaned with tap water and oven (SL 1375 SHEL LAB 1350 FX) dried at 105°C for 6 h. The dried PFW was carbonized at 500°C with an increment rate of 10°C min^{-1} and then kept at constant temperature for 1 h. The obtained Pineapple Fiber Waste Carbon (PFWC), which consists of 3.55% ash, 68.27% C, 22.61% O, 1.62% Si, 1.66% P, 3.87% K and 1.96% Ca, was modified with $KMnO_4$ (Merck, Germany) using 1, 3, or 5 %wt ratios. $KMnO_4$ modified Pineapple Fiber Waste Carbon (KPFWC) was oven (SL 1375 SHEL LAB 1350 FX) dried at 105°C for 3 h and then used for Fe^{3+} adsorption experiments.

Analysis and Characterization

The modified products (KPFWC) were characterized by a Fourier transform infrared spectrometer (Spectrum GX, Perkin Elmer), X-ray diffractometer (PW 3040/60, X' Pert Pro MPD), scanning electron microscope-energy dispersive X-ray spectrometer (PHILIPS LEO 1455 VP) and Brunauer Emmett Teller surface area analyzer (Micromeritics TriStar II). The ash content of all samples was also analyzed by standard methods (ASTM, 1996).

SEM-EDS Analysis

Scanning electron microscopy was used to visualize the surface morphology of samples. The samples were coated with gold by a gold sputtering device for a clear vision of the surface morphology. Elemental composition of the samples was also observed using energy dispersive spectrometer by scanning through the surface of the samples.

XRD Analysis

X-ray patterns of modified products were recorded by X-ray powder diffractometer with a Cu tube anode.

FTIR Analysis

The distribution of surface functional groups of the samples was studied using a Fourier transform infrared spectrometer in the range 400-4000 cm^{-1}. The samples were prepared as pellets in IR grade KBr (Yang *et al*., 2011).

BET Measurement

Textural characteristics of samples were determined by N_2 adsorption at -196°C on a Brunauer Emmett Teller surface area analyzer. The samples were degassed at 250°C for 12 h under vacuum before the measurements. The multipoint Brunauere Emmette Teller equation was used to estimate the specific surface areas.

Fe Adsorption Experiments

The 1000 mg dm^{-3} Fe^{3+} stock solution was prepared from 0.4827 g of $FeCl_3 \cdot 6H_2O$ (Merck, Germany) was dissolved in deionized water, acidified with 1 cm^3 of 1 M HCl added and then diluted to 100 cm^3 with deionized water. Further solutions (5 mg dm^{-3}) were prepared from the stock solution by dilution.

Fe^{3+} adsorption experiments were followed using a method of Üçer *et al*. (2005). A KPFWC with 1 wt% was added to 50 cm^3 of Fe^{3+} solution (5 mg dm^{-3}) in a conical flasks and shaken continuously at 120 rpm at a temperature of 32±2°C. Following the adsorption, the aqueous phase was separated by centrifugation at 4000 rpm for 10 min and the final Fe^{3+} ion concentration in the solution was determined by FAAS (Varian Spectr AA 220, Australia) with air-acetylene and cathode on Fe-hollow cathode lamp at 248.3 nm.

The amount of Fe^{3+} removal was calculated by the difference in initial and final concentrations. The optimum condition for Fe^{3+} removal was determined at different effects (e.g., pH 2-9, contact time (20-180 min) and KPFWC loading (0.05-2.0 g)).

Final concentration (C_f) of Fe^{3+} was measured and calculated of Fe^{3+} removal percentage as shown in the following equation (Shrestha *et al*., 2013):

$$\text{Removal } \% = \left(\left(C_o - C_f\right) / C_o\right) \times 100 \quad (1)$$

Where:
C_o = The initial Fe^{3+} concentration (mg dm^{-3})
C_f = The final Fe^{3+} concentration (mg dm^{-3})

The adsorption capacity (q_t, mg g^{-1}) at any time was calculated as shown below (Shrestha *et al*., 2013):

$$q_t = \left(C_o - C_f\right) \times \left(V / W\right) \quad (2)$$

Where:
V = The volume of the solution (dm^3)
W = The mass of dry adsorbent used (g)

Adsorption Isotherms

All of the experimental adsorption data's were fitted with both Langmuir equation and Freundlich equation.

The Langmuir equation is:

$$Q_e = \left(q_{max} K_L C_e\right) / \left(1 + K_L C_e\right) \quad (3)$$

Where:
Q_e (mg g^{-1}) = The Fe^{3+} adsorbed amount per unit mass of adsorbent
C_e (mg dm^{-3}) = The Fe^{3+} equilibrium concentration
q_{max}(mg g^{-1}) = The maximum Fe^{3+} amount that forms a complete monolayer on the surface of adsorbent
K_L (dm^3 mg^{-1}) = The Langmuir constant which associated to adsorption heat

The linear form of this equation after rearrangement is:

$$C_e / Q_e = 1 / q_{max} K_L + C_e / q_{max} \quad (4)$$

The constants q_{max} and K_L was determined from the slope and intercept of plotting C_e/Q_e against C_e, respectively (Mahmoud, 2015).

Freundlich model is used to estimate the adsorption intensity of KPFWC towards the Fe^{3+} ions and is:

$$Q_e = K_F C_o^{(1/n)} \quad (5)$$

This equation is conveniently used in linear form as (Mahmoud, 2015):

$$\text{Log } Q_e = \text{Log } K_F + 1/n \,\text{Log } C_e \quad (6)$$

where, Q_e and C_e have the same definitions of the Langmuir equation. K_F and n are Freundlich constants related to adsorption capacity and heterogeneity factor, respectively. The constants K_F and n were determined from the slope and intercept of plotting Log C_e against Log Q_e, respectively.

Results and Discussion

SEM and EDS Analyses

The SEM image of PFW (non fiber part) (Fig. 1a) exhibits a notched surface, while 3% $KMnO_4$ modified fresh pineapple waste (3KPFW) (Fig. 1b) displays a smooth surface. This reveals that $KMnO_4$ covered the surface of PFW after $KMnO_4$ modification. Figure 1c shows the image of PFWC after carbonization at 500°C. It can be seen that the PFWC is in a furrow form with a fairly smooth surface. However, the images modified pineapple waste (3KPFWC) after carbonization at 500°C and modification with 3 %wt of $KMnO_4$ (Fig. 1d-e) display a rougher surface with cracks and a large number of small particles. This is because the PFW was significantly oxidized by $KMnO_4$, degraded and became brittle and opaque (Fávaro *et al*., 2007). The small particles are quite non-uniformly dispersed on the surface of KPFWC. These particles are rich in K and Mn content as determined by point analysis using EDS (Table 1). This analysis also confirmed that C, O, Si, K and Mn are the main composition in the all of the KPFWC materials. Furthermore, it indicated that MnO_2 deposited on the surface of KPFWC. The high amounts of K and Mn elements on the surface of KPFW and KPFWC after carbonization at 500°C indicated that $KMnO_4$ is fixed on the surface of modified waste with massively (Kaushik, 2000).

Table 1. Elemental composition of samples determined by EDS analysis

	wt% of elements				
Samples	C	O	Si	K	Mn
PFW	49.03	45.54	1.16	0.93	0.93
PFWC at 500°C	68.27	22.61	1.62	3.87	3.87
1KPFW	74.82	15.61	0.93	3.05	1.03
3KPFW	73.44	13.85	4.71	6.13	1.87
5KPFW	62.38	17.11	1.87	6.90	5.80
1KPFWC at 500°C	74.55	13.83	1.53	3.04	2.06
3KPFWC at 500°C	59.56	17.14	6.82	8.65	7.82
Point on particle on surface of 3KPFWC at 500°C	37.61	8.46	14.63	19.99	19.85
5KPFWC at 500°C	43.36	7.62	2.11	24.75	11.36

DOI: 10.3844/ajassp.2016.814.826

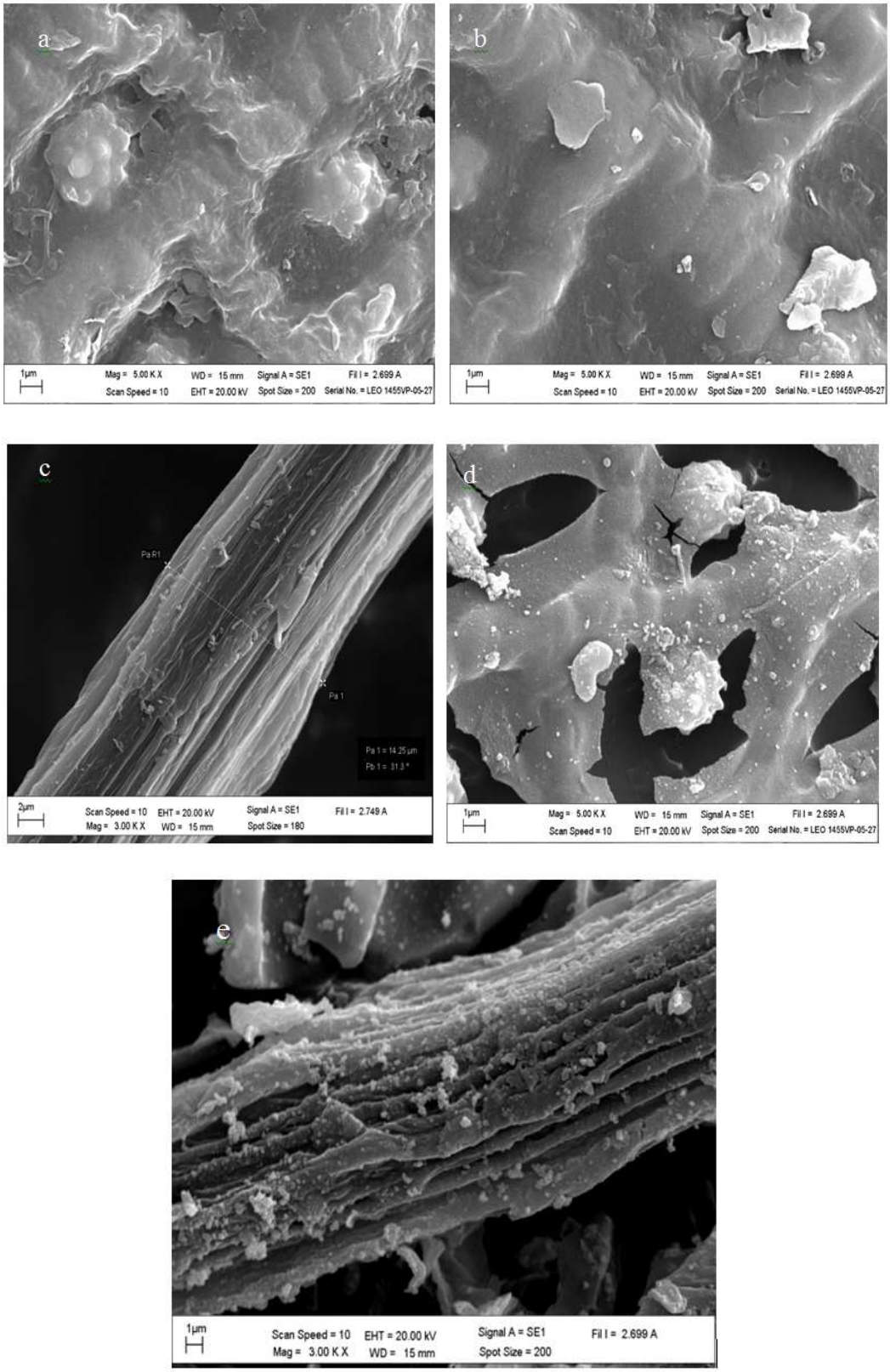

Fig. 1. SEM images of (a) PFW, (b) 3KPFW, (c) PFWC (carbonized at 500°C), (d) 3KPFWC (carbonized at 500°C) and (e) 3KPFWC (carbonized at 500°C)

DOI: 10.3844/ajassp.2016.814.826

XRD Results

Figure 2a showed the XRD spectrum of PFW. It exhibits the diffraction peaks of cellulose at 2θ of about 15-17 and 22° (Hajji *et al*., 2016). On the other hand, the XRD spectra of PFWC after carbonization at 500°C (Fig. 2b) show amorphous phase of carbon with broad peaks at 24 and 43°. These spectra also contain a peak at 29.5° and a little peak at 34.5°, which were related to a calcium and a potassium compound, respectively (Mopoung and Amornsakchai, 2016). This indicates that the crystalline cellulose has decomposed into amorphous materials during the carbonization process (Hajji *et al*., 2016). For 1KPFWC obtained after carbonization at 500°C (Fig. 2c), the diffraction peaks at about 22, 37, 42, 57 and 66° show the presence of MnO_2 in an amorphous phase (Wang *et al*., 2012; Xie and Gao, 2007). The MnO_2 was generated by the reduction of $KMnO_4$ in acid solution (Fávaro *et al*., 2007). These results confirm that the interaction between $KMnO_4$ and PFW has occurred. In addition, a Si phase is also observed at about 28.5, 47 and 69° (Zhang *et al*., 2016), which probably comes from the original waste material.

Spectra FTIR

Figure 3a shows the FTIR transmission spectrum of PFW. It exhibits the peaks of cellulose, which consist of a strong board band at 3200-3400 cm^{-1} (ν(OH) vibration of the intra molecular hydrogen bond from cellulose) (Habibi, 2014), weak peaks at 2850.8-2918.8 cm^{-1} (*ν*(CH) vibration) (Hajji *et al*., 2016), 1737.3 cm^{-1} (*ν*(C = O) vibration in the cellulose chain) (Hajji *et al*., 2016), 1635 cm^{-1} (*δ*(OH) vibration of adsorbed water in crystalline cellulose (Zhao *et al*., 2013) or COO^- stretching (Zhao *et al*., 2013), 1515.6 cm^{-1} (*ν*(CO) group and aromatic skeletal stretching of lignin (Zhao *et al*., 2013), 1431.3 cm^{-1} (*δ*(CH_2) deformation vibrations) (Hajji *et al*., 2016), 1373 cm^{-1} (*δ*(CH) in plane deformation vibrations in lignin, (Zhao *et al*., 2013), 1323 cm^{-1} (*δ*(CH_2) vibrations associated to crystallized cellulose I composition), 1235 cm^{-1} (ν(C-O) vibration) (Zhao *et al*., 2013), 1160.4 cm^{-1} (*ν*(C–O–C) vibration of the *β*-(1-4)-glycosidic linkage) (Hajji *et al*., 2016) or *ν*(C–OH) groups (Habibi, 2014), very weak peak 1106 cm^{-1} (asymmetric stretching of the glycosidic ring or *ν*(C–Si–O)) (Gong *et al*., 2016), 1056.3 cm^{-1} (*ν*(C–O) vibration of secondary alcohol), indicating the presence of lignin in the waste (Mokhtari and Faghihian, 2015), 1026 cm^{-1} (*ν*(C–O) vibrations of primary alcohol) and 897 cm^{-1} (C–O–C bonds in the glycosidic linkage of crystalline cellulose) (Hajji *et al*., 2016) and the band between 610-527 cm^{-1} (C–O deformation vibration (Zhang *et al*., 2013a)). These peaks disappear after $KMnO_4$ modification for both carbonized and non-carbonized materials (Fig. 3b-n), with the exception of peaks at 1373, 1235 and 1090 cm^{-1}. These functional groups were not observed in carbonized samples (Fig. 3e-n) as they undergo thermal degradation (Hajji *et al*., 2016). Thermal degradation by dehydration occurs above 140°C and dehydroxylation takes place above 550°C. At temperatures in the range of 160-230°C, water molecules which as physically adsorbed and belong in interlayer of adsorbent are removed. Increasing the temperature to 350°C causes the degradation of hydroxyl, carboxyl and carbonyl groups of cellulose (Luo *et al*., 2013; Natkański *et al*., 2013). For 1, 3, 5% KPFW and KPFWC (Fig. 3b-d), the results are attributed to the surface of materials being covered by MnO_2 (Xie and Gao, 2007). So, the functional groups on these samples are shielded.

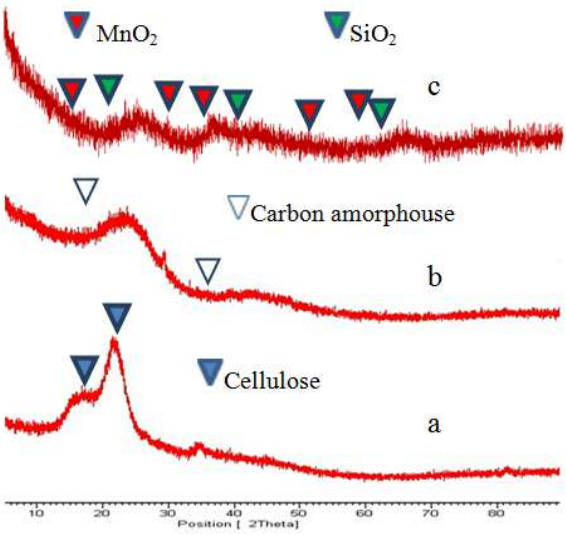

Fig. 2. XRD diffractogrames of PFW (a), PFWC (carbonized at 500°C) (b) and 1KPFWC (carbonized at 700°C) (c)

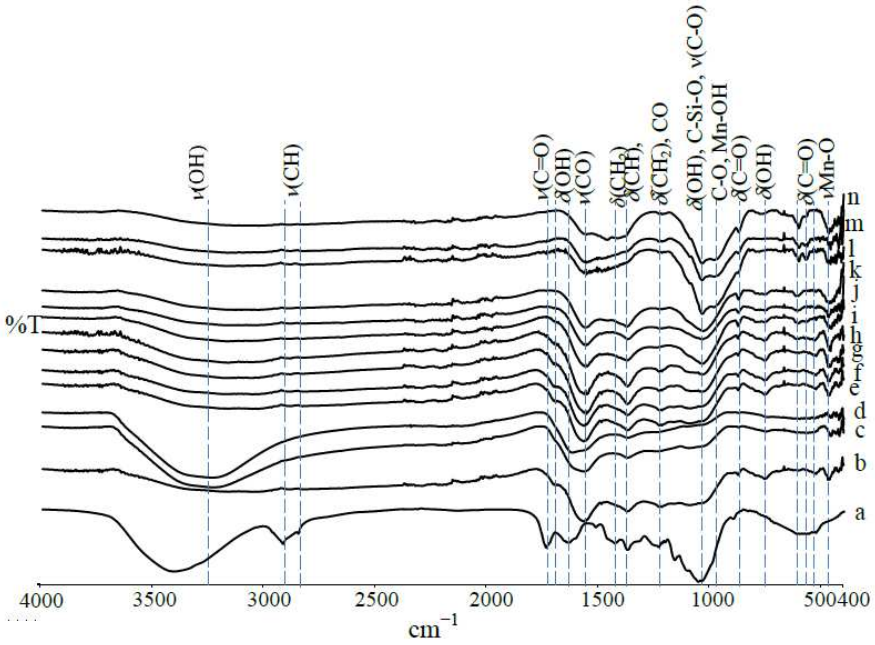

Fig. 3. FTIR transmission spectra of 0, 1, 3 and 5 KPFW (a-d), 0,1,3,5 KPFWC (carbonized at 500°C) (e-h), 1,3,5 KPFWC (carbonzied at 600°C) (i-k) and 1,3,5 KPFWC (cabonizedat 700°C) (l-n), respectively

The remaining peaks at 1373, 1235 and 1090 cm^{-1} are in $KMnO_4$ modified samples. The peak at 1373 cm^{-1} is associated with H–O bending vibration in phenols and carboxyls after $KMnO_4$ oxidation (Chen *et al*., 2012). The weak peak at 1235 cm^{-1} is related to C–O in phenols. The presence of this peak provides evidence of oxidization of the waste materials by $KMnO_4$ to generate phenols (Chen *et al*., 2012). The peak of *ν*C–O vibration at 1090 cm^{-1}, which is slightly shifted from 1106 cm^{-1}, could also be associated to *δ*O–H vibrations which bound to Mn atoms (Xie and Gao, 2007). This peak could also be attributed to stretching vibration of C–Si–O moiety (Gong *et al*., 2016).

The board peak of ν(OH) at 3156-3227 cm^{-1} in KPFW and KPFWC (Fig. 3b-n), which is shifted from the value of 3402 cm^{-1} in PFW, is attributed to *ν*H-O vibration in phenols and carboxyls, which were formed by $KMnO_4$ oxidation (Chen *et al*., 2012). This peak decreases in intensity with increasing carbonization temperature and disappears completely for samples carbonized at 700°C and above. This corresponds to the dehydration and desorption of cellulose and water molecules, respectively, which acted as a hydrogen bonding network of intra and intermolecular cellulosic chains (Hajji *et al*., 2016). It has been seen that the board peak at 3156-3227 cm^{-1} in KPFW disappeared after modification with 1% $KMnO_4$ modified (Fig. 3b). However, a boarder peak appears in the same position after modification with 3-5% $KMnO_4$ (Fig. 3c-d). This is because the content of carboxylic acids increases after oxidation at high $KMnO_4$ concentration (Chen *et al*., 2012). Therefore, *ν*H–O vibration of carboxyl groups is enhanced after modification with 3-5% $KMnO_4$. However, this peak disappeared in 1KPFW. This is attributed to the functional groups being obscured by MnO_2 at low $KMnO_4$ concentration as has been observed previously by Xie and Gao (2007). The new peaks appearing after $KMnO_4$ modification in KPFW and KPFWC materials are present at about 1560, 1035, 872, 755, 550 and 460 cm^{-1}. The peak at 1560 cm^{-1} is associated to conjugated *ν*C–O vibration. This peak decreases in intensity with increasing carbonization temperature and $KMnO_4$ concentration. It indicates that the modified samples contain a small amount of carboxyl groups. This is caused by the presence of C = C moieties with red-shift characteristic of oxygen-rich surfaces leading to the diminution of the C = O peak (Ma *et al*., 2009). The peak at 1035 cm^{-1} (associated to C–O vibration), which is shifted from the normal value of 1056 cm^{-1}, also increased in intensity with increasing carbonization temperature due to oxidation by $KMnO_4$. This is especially true at 700°C, where it has high intensity and a shoulder peak at 980 cm^{-1}. This is likely due to the overlapping of C–O stretching and Mn–OH vibration (Ma *et al*., 2009). The very weak peak at 872 cm^{-1}, which is shifted from the normal value of 897 cm^{-1}, corresponds to the *δ*O–H bonds, which also result in a board peak at 3156-3227 cm^{-1}. The weak peak at 755 cm^{-1} is corresponding to the *δ*C = O bond on the aromatic rings, which forms by substitution (Fávaro *et al*., 2007) after $KMnO_4$ modification. The peak at about 550 cm^{-1} in the spectra of 1-5 KPFW and 1-5KPFWC

carbonized at 500°C are associated to the vibration of Mn–O bond (Zhang *et al*., 2015). In addition, the peak at 460 cm^{-1}, which is also associated to the *v*Mn–O bond vibration, indicates that Mn has been successfully existed on surface of the waste materials (Wang *et al*., 2012). The weak peaks at about 600 cm^{-1}, appearing in samples prepared with carbonization at 500°C and above, increase in intensity with increasing carbonization temperature from 500 to 700°C. These peaks are attributed to C–O deformation vibrations, which likely arise from $KMnO_4$ addition (Zhang *et al*., 2013b). The OH and CO groups on the surface of samples are result of the $KMnO_4$ modification process (Ma *et al*., 2009), since $KMnO_4$ can oxidize unstable groups such as phenols, lactones, or lactols into carboxyls (Chen *et al*., 2012). These functional groups on $KMnO_4$ modified waste prepared with carbonization act as the initiation points for adsorbing external materials (Luo *et al*., 2013).

BET Measurement

Table 2 shows the BET surface area, pore volume and average pore size of PFW, PFWC (carbonized at 500°C), 1-3 KPFW and 1-3 KPFWC (carbonized at 500°C). It showed that the BET surface area and total pore volume of 1-3 KPFW and 3 KPFWC (carbonized at 500°C) are increased in comparison to PFW and PFWC (carbonized at 500°C). This was due to the addition of $KMnO_4$. On the other hand, the average pore size decreased after $KMnO_4$ modification and carbonization. The results suggest that $KMnO_4$ treatment can improve the porosity of the waste materials by oxidation process, which can enlarge the pores of the materials (Wang *et al*., 2012). It can be seen that the BET surface area and total pore volume of 3KPFW is lower than of 1KPFW. But the average pore size trends in the opposite direction. This is because of the formation of oxygen-containing functional groups and MnO_2 blocking the pore entrances (Luo *et al*., 2013), thereby decreasing the surface area and pore volume of 3KPFW. However, 3KPFW is still oxidized to a higher extent than 1KPFW. Therefore, the average pore size of 3KPFW is higher than 1KPFW. For 3KPFWC obtained after carbonization at 500°C, the results are due to extensive thermal oxidation with $KMnO_4$, which increases the surface area and pore volume. Meanwhile, the micropores and mesopores are formed to a greater extent resulting in decreased average pore size (Wang *et al*., 2012).

Effect of $KMnO_4$ Modification of Waste Materials on Fe^{3+} Removal

The Fe^{3+} removal by PFWC and 1KPFWC were compared (Fig. 4). The experiments were carried out using 0.1 g of PFWC or 1KPFWC loaded in 50 cm^3 of 5 mg dm^{-3} Fe^{3+} solutions at pH 5 for 60 min contact time. The results show that the Fe^{3+} ion removal can be improved by material modification with $KMnO_4$. This is due to the high content of MnO_2 and carboxylic functional groups in the modified materials. The modified material 1KPFWC has exhibited relatively high Fe^{3+} removal capacity (98.2% or 2.455 mg g^{-1}). The Fe^{3+} ion removal capacity of 1KPFWC was approximately 4.5 times higher than that of PFWC. This indicates that KPFWC provides more binding sites for Fe^{3+} than PFWC. This could be explained by Fe^{3+} being attracted by electrostatic force to MnO_2 or other functional groups e.g., carboxylate groups, on KPFWC which can be protonated and deprotonated (Natkański *et al*., 2013). It is the result of complex formation of Fe^{3+} and functional groups on modified material (Hu *et al*., 2015).

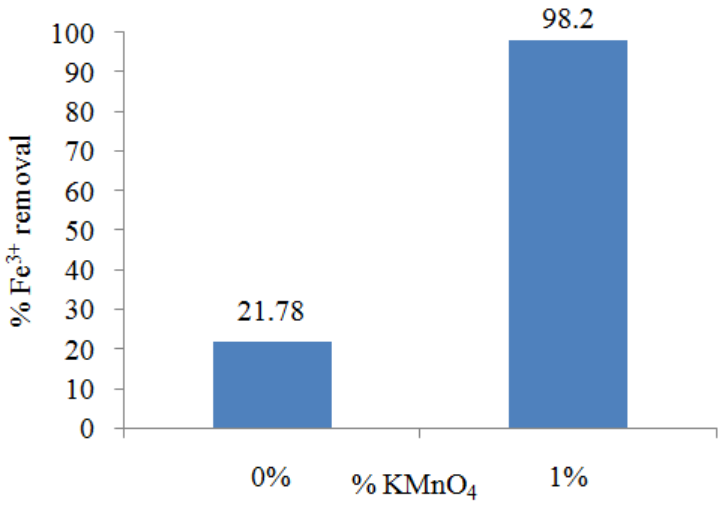

Fig. 4. Comparison of Fe^{3+} removal efficiency of 1KPFWC and PFWC

Table 2. BET surface area, pore volume and average pore size of the samples

Samples	BET surface area ($m^2 g^{-1}$)	Pore volume ($cm^3 g^{-1}$)	Average pore size (nm)
PFW	48.4335	0.03076	2.5402
PFWC at 500°C	106.7863	0.06708	2.5126
1KPFW	142.8920	0.07356	2.0594
3KPFW	115.1215	0.06359	2.2095
3KPFWC with 500°C carbonized	167.4968	0.08698	2.0772

Effect of Contact Time on Fe^{3+} Removal

Figure 5 shows the effect of contact time (0-180 min) on Fe^{3+} removal at pH 7 using 0.1 g of 1KPFWC in 50 cm^3 of 5 mg dm^{-3} Fe^{3+} ion solution. The results show that the Fe^{3+} adsorption rate is quite fast and reaches to equilibrium state after about 60 min. The initial rapid adsorption is due to the availability of high amount of vacant sites on surface of the adsorbent. At later stages the vacant sites which were adsorpted, becomes difficult more adsorpted. This is caused by repulsive forces between Fe^{3+} ions adsorbed on the 1KPFWC surface and Fe^{3+} ions in solution (Liu *et al*. 2015). Increasing of the adsorption efficiency with increasing the contact time has two functions. Firstly, the swelling of the adsorbent is increases, which increases its contact surface. The swelling property could result in higher hydrophilicity of the adsorbent (Natkański *et al*., 2013). Secondly, the contact between the swelled adsorbent and the metal ions is also increases, which increases the availability of interaction between the active functional groups on the surface of adsorbent and the metal ions in solution. As the result, the amount of metal ions adsorbed by surface functional groups increases, which increases metal ion uptake (Sadeek *et al*., 2015). It can be seen that the efficiency Fe^{3+} adsorption is quite low. This is because this experiment was carried out at pH 7, which is not optimal condition. Based on these results, the contact time for further experiments was fixed at 60 min.

Effect of pH Value on Fe^{3+} Removal Efficiency

The effect of pHs (2-9) on the efficiency of Fe^{3+} ion removal by 0.1 g of 1KPFWC was investigated using 50 cm^3 of 5 mg dm^{-3} solution of Fe^{3+} ions with 60 min contact time. The results of this experiment are shown in Fig. 6. The amount of Fe^{3+} adsorbed on the 1KPFWC increased with increasing pH and reached maximum at pH of about 4.7. This value is similar to the value found for carboxymethylated chitosan hydrogels (Wang *et al*., 2008). The adsorption efficiency then decreased with further increases in pH. The Fe^{3+} adsorption efficiency decreased gradually at pH values between 5-6. This was followed by a sharp decline at pH >7.

The adsorption reaction of MnO_2 groups on the material surface leading to Fe^{3+} adsorption can be elucidated by Equation 7 and 8 (Hu *et al*., 2015):

$$MnOH \rightleftharpoons MnO^- + H^+ \quad (7)$$

where, MnOH and MnO^- are the protonated and deprotonated MnO_2 sites, respectively:

$$MnO^- + Fe^{3+} \rightleftharpoons MnO^-Fe^{3+} \quad (8)$$

These reactions result in the formation of the $[MnOFe]^{2+}$ complex.

The solution pH affects to the form of Fe^{3+} ions in solution and the properties of the adsorbent surface in terms of dissociation of functional groups and surface charges (Liu *et al*., 2015). At very low pH values, the concentration of H^+ is much higher than that of Fe^{3+} ions, which increases the competition between H^+ ions and Fe^{3+} ions for the surface sites of the modified waste materials. Therefore, the functional groups on 1KPFWC would preferentially combine with H^+ making the surface positively charged, which is disadvantageous for the interaction between 1KPFWC and Fe^{3+} ions. At higher pH values, the amount of protonated functional groups on the $KMnO_4$ modified waste materials would decrease and Fe^{3+} ions would thus have more opportunities to compete with H^+ for binding with surface functional groups of 1KPFWC (He *et al*., 2014). This greatly improves Fe^{3+} adsorption. Therefore at pH below 4.7, the adsorption capacity for Fe^{3+} ions on 1KPFWC is low. The highest Fe^{3+} adsorption capacity of 1KPFWC was observed to be about 90% at the pH value of 4.7. However, at higher pH values (>5), the adsorption efficiency for Fe^{3+} ions decreases. This is especially true at pH >7, where the Fe^{3+} ions in the solution exist in from of $Fe(H_2O)_6]^{3+}$, which can react with hydroxide ions to form the insoluble $Fe(OH)_3$ (Lee *et al*., 2006). The formation of this species inhibits the adsorption process significantly. As a result the Fe^{3+} adsorption amount decreases. Thus pH value of about 5 is suitable for the adsorption of Fe^{3+} ions.

Effect of Modified Waste Loading on Fe^{3+} Removal

Figure 7 shows the Fe^{3+} removal with 0.05-2.0 g of 1KPFWC loaded in 50 cm^3 of 5 mg dm^{-3} Fe^{3+} solution, at pH 5 and with 60 min contact time. The results show that the Fe^{3+} removal efficiency reaches the maximum (98.2%) with only 0.1 g of 1KPFWC. With loading in the range of 0.5-2.0 g the adsorption efficiency is maintained. On the other hand, with 1KPFWC loading below 0.05 g low Fe^{3+} removal efficiency is occurred, due to the adsorption surface saturation (Lee *et al*., 2006) of 1KPFWC. Therefore, the loading amount of 1KPFWC was fixed at 0.1 g for subsequent experiments.

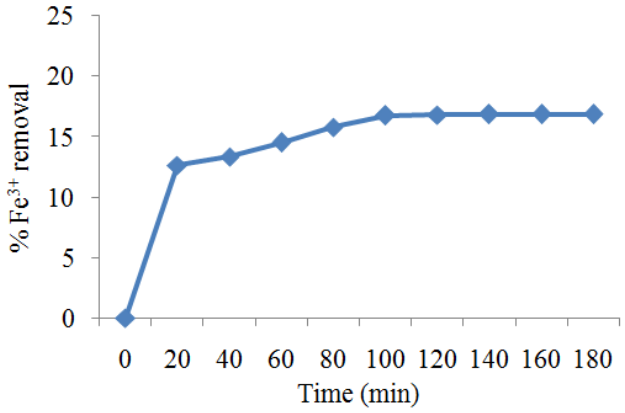

Fig. 5. Effect of contact time on Fe^{3+} removal efficiency

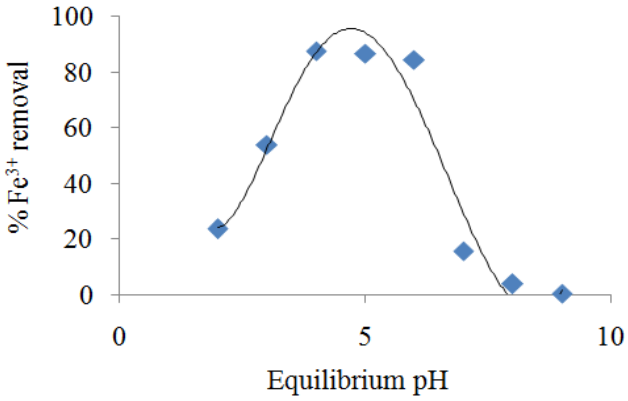

Fig. 6. Effect of pH on Fe^{3+} removal efficiency

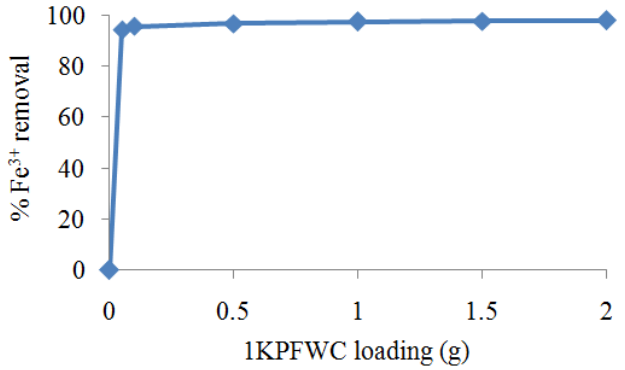

Fig. 7. Effect of 1KPFWCloading on Fe^{3+} removal efficiency

Isotherm of Fe^{3+} Ion Adsorption

Fe^{3+} ion adsorption isotherm studies were carried out with 0.05-2.0 g of 1KPFWC loaded in 50 cm^3 of 5 mg dm^{-3} Fe^{3+} solution, at pH 5 and with 60 min contact time. Langmuir isotherm and Freundlich isotherm are used to correlate the Fe^{3+} adsorption equilibrium data. Both the Langmuir isotherm (Fig. 8) and Freundlich isotherm (Fig. 9) were fitted using the experimental data, as was done by Yang *et al*. (2014). The R^2 values of these linear isotherms are nearly equivalent, with the values of 0.9919 and 0.9924 for Langmuir isotherm and Freundlich isotherm, respectively. Thus, the Freundlich adsorption model appears slightly better than the Langmuir model. It was shown that the Fe^{3+} ion adsorption occurrs on the heterogeneous surface of 1KPFWC. However, at low Fe^{3+} concentration it only takes place in a monolayer without interaction between Fe^{3+} ions and with no transmigration on the surface of 1KPFWC (Liu *et al*., 2013).

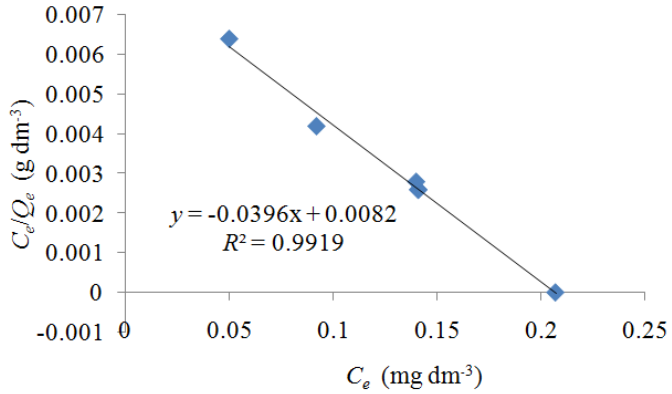

Fig. 8. Fe^{3+} adsorption Langmuir isotherm plot for 1KPFWC

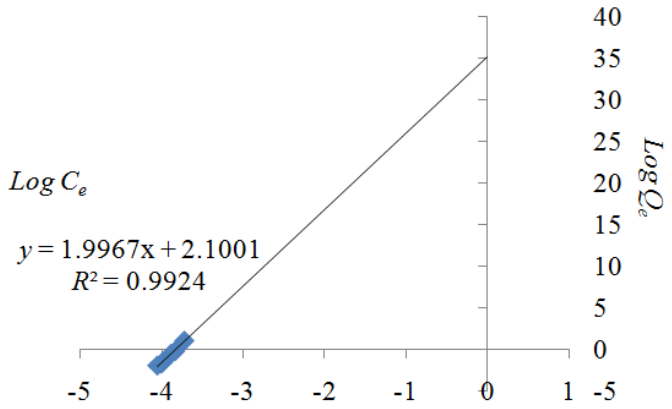

Fig. 9. Fe^{3+} adsorption Freundlich isotherm plot for 1KPFWC

It can be seen from the SEM image of 1KPFWC (Fig. 3d and e) that its surface is rough with cracks and a large number of non-uniform small particles and many functional group types (Fig. 3), which indicates a heterogeneous surface (Dissanayake *et al*., 2016). According to the Langmuir equation, the maximum Fe^{3+} adsorption capacity (q_{max}) and Langmuir constant (K_L) values were calculated by linear regression. The theoretical maximum adsorption capacity value and K_L for Fe^{3+} ions on 1KPFWC were 25.25 mg g^{-1} and 0.2071 dm^3 g^{-1}, respectively. An estimation of the dimensionless factor R_L from the values of C_0 and K_L was obtained using the relationship $R_L = 1/(1+ K_L C_0)$. The value of R_L is 0.4912, which in the range $0<R_L<1$. Therefore, 1KPFWC appears to be suitable for Fe^{3+} ions adsorption (Liu *et al*., 2013). In addition, Freundlich model provides two parameters K_F and n from the slope and intercept of the plot of Log *Qe* against Log *Ce* in Fig. 9. The K_F and n values are 125.92 $dm^{3(1/n)}$ $mg^{(1-1/n)}$ g^{-1} and 0.5008, respectively. The K_F value is quite high, which represents a high Fe^{3+} ion adsorption capacity on the modified waste carbon material. But n value is< 1, which indicates relatively low heterogeneity of the adsorbent (Mahmoud, 2015).

Conclusion

The $KMnO_4$ modified carbon materials obtained from waste of pineapple fiber production processing were characterized by SEM-EDS, XRD, FTIR and BET. The results from SEM-EDS show a rougher surface with cracks and a large number of small particles with major content of C, O, Si, K and Mn elements in the all of KPFWC materials. The results of the XRD confirmed that MnO_2 was deposited on the surface of $KMnO_4$ modified waste carbon materials. In addition, the results from the FTIR analysis revealed that the OH, CO and MnO_2 groups are the major functional groups on the surface of $KMnO_4$ modified carbon materials. The BET surface area and total pore volume of modified waste carbon materials increases with increasing weight % of $KMnO_4$ used in the modification and increasing carbonization temperature. On the other hand, the average pore size follows an inverse trend. This is due to the formation of oxygen-containing functional groups and MnO_2, which block the pore entrances. It was shown that the Fe^{3+} adsorption on modified waste carbon materials reaches equilibrium within 60 min and that the amount of Fe^{3+} adsorbed increases with increasing pH up

to the optimal value of 4.7. The adsorption efficiency then decreases, with a sharp decrease observed at pH values >7. Both Langmuir isotherm model and Freundlich isotherm model can be fitted to the Fe^{3+} adsorption data with high R^2 values of 0.9919 and 0.9924, respectively. The theoretical maximum adsorption capacity of Fe^{3+} on the modified waste carbon materials was estimated as 25.25 mg g^{-1}. The materials also show some heterogeneity on their surfaces, which is favorable for Fe^{3+} ion adsorption**.** Therefore it can be concluded that pineapple fiber leaf wastes from pineapple fiber production processing, which are cheap, easily available and can be used more economically on large scale, have high potential for conversion to Fe^{3+} ion adsorbents by modify with $KMnO_4$.

Acknowledgement

The authors acknowledge the Chemistry Department and Science lab center, Faculty of Science, Naresuan University for all of the analysis.

Funding Information

This work was financially supported by Naresuan University.

Author's Contributions

Sumrit Mopoung: Designed the research plan, organized the study and wrote of all paragraphs.

Thaksaphon Bunterm: Co-researcher who has reported and analysed data of this paper.

Ethics

This article is original and contains unpublished material. The corresponding author confirms that all of the other authors have read and approved the manuscript and no ethical issues involved.

References

Abecassis-Wolfovich, M., R. Jothiramalingam, M.V. Landau, M. Herskowitz and B. Viswanathan *et al*., 2005. Cerium incorporated ordered manganese oxide OMS-2 materials: Improved catalysts for wet oxidation of phenol compounds. Applied Catalysis B: Environ., 59: 91-98. DOI: 10.1016/j.apcatb.2005.01.001

ASTM, 1996. Standard test method for total ash content of activate carbon. American Standard of Testing Material.

Arulraj, J. and M. Rajamathi, 2013. Preparation of anionic clay-birnessite manganese oxide composites by interlayer oxidation of oxalate ions by permanganate. J. Solid State Chem., 198: 303-307. DOI: 10.1016/j.jssc.2012.10.014

Baccar, R., J. Bouzid, M. Feki and A. Montiel, 2009. Preparation of activated carbon from Tunisian olive-waste cakes and its application for adsorption of heavy metal ions. J. Hazardous Mater., 162: 1522-1529. DOI: 10.1016/j.jhazmat.2008.06.041

Chen, J., O. Chen, Q. Ma, Y. Li and Z. Zhu, 2012. Chemical treatment of CNTs in acidic $KMnO_4$ solution and promoting effects on the corresponding Pd–Pt/CNTs catalyst. J. Molecular Cataly. A: Chem., 356: 114-120. DOI: 10.1016/j.molcata.2011.12.032

Daifullah, A.A.M., S.M. Yakout and S.A. Elreefy, 2007. Adsorption of fluoride in aqueous solutions using $KMnO_4$-modified activated carbon derived from steam pyrolysis of rice straw. J. Hazardous Mater., 147: 633-643. DOI: 10.1016/j.jhazmat.2007.01.062

Dissanayake, D.M.R.E.A., W.M.K.E.H. Wijesinghe, S.S. Iqbal and N. Priyantha, 2016. Isotherm and kinetic study on Ni(II) and Pb(II) biosorption by the fern *Asplenium nidus L*. Ecol. Eng., 88: 237-241. DOI: 10.1016/j.ecoleng.2015.12.028

Fávaro, S.L., A.F. Rubira, E.C. Muniz and E. Radovanovic, 2007. Surface modification of HDPE, PP and PET films with $KMnO_4$/HCl solutions. Polymer Degradat. Stability, 92: 1219-1226. DOI: 10.1016/j.polymdegradstab.2007.04.005

Gong, Z., S. Li, J. Ma and X. Zhang, 2016. Self-flocculated powdered activated carbon with different oxidation methods and their influence on adsorption behavior. J. Hazardous Mater., 304: 222-232. DOI: 10.1016/j.jhazmat.2015.10.039

Habibi, N., 2014. Preparation of biocompatible magnetite-carboxymethyl cellulose nanocomposite: Characterization of nanocomposite by FTIR, XRD, FESEM and TEM. Spectrochimica Acta Part A: Molecular Biomolecular Spectroscopy, 131: 55-58. DOI: 10.1016/j.saa.2014.04.039

Hajji, L., A. Boukir, J. Assouik, S. Pessanha and J.L. Figueirinhas *et al*., 2016. Artificial aging paper to assess long-term effects of conservative treatment. Monitoring by infrared spectroscopy (ATR-FTIR), X-Ray Diffraction (XRD) and Energy Dispersive X-Ray Fluorescence (EDXRF). Microchem. J., 124: 646-656. DOI: 10.1016/j.microc.2015.10.015

He, Z., H. Song, Y. Cui, W. Zhu and K. Du *et al*., 2014. Porous spherical cellulose carrier modified with polyethyleneimine and its adsorption for Cr(III) and Fe(III) from aqueous solutions. Chinese J. Chem. Eng., 22: 984-990. DOI: 10.1016/j.cjche.2014.07.001

Hu, Q., Z. Xiao, X. Xiong, G. Zhou and X. Guan, 2015. Predicting heavy metals' adsorption edges and adsorption isotherms on MnO_2 with the parameters determined from Langmuir kinetics. J. Environ. Sci., 27: 207-216. DOI: 10.1016/j.jes.2014.05.036

Kaushik, V.K., 2000. Surface characterization of $KMnO_4$ treated carbon fiber precursors using X-ray photoelectron spectroscopy. Polymer Test., 19: 17-25. DOI: 10.1016/S0142-9418(98)00068-3

Kengkhetkit, N. and T. Amornsakchai, 2012. Utilisation of pineapple leaf waste for plastic reinforcement: 1. A novel extraction method for short pineapple leaf fiber. Indus. Crops Products, 40: 55-61. DOI: 10.1016/j.indcrop.2012.02.037

Lee, H.J., D.W. Kang and Y.J. Lee, 2006. Removal of metals and organics in a chemical decontamination process solution: Laboratory and semi-pilot scale experiments. Chem. Eng. J., 116: 219-225. DOI: 10.1016/j.cej.2005.09.027

Liang, S.H., K.F. Chen, C.S. Wu, Y.H. Lin and C.M. Kao, 2014. Development of $KMnO_4$-releasing composites for in situ chemical oxidation of TCE-contaminated groundwater. Water Res., 54: 149-158. DOI: 10.1016/j.watres.2014.01.068

Liu, J., H.T. Wu, J. Lu, X. Wen and J. Kan *et al*., 2015. Preparation and characterization of novel phenolic acid (hydroxybenzoic and hydroxycinnamic acid derivatives) grafted chitosan microspheres with enhanced adsorption properties for Fe(II). Chem. Eng. J., 262: 803-812. DOI: 10.1016/j.cej.2014.10.041

Liu, J., X. Gao, C. Liu, L. Guo and S. Zhang *et al*., 2013. Adsorption properties and mechanism for Fe(III) with solvent impregnated resins containing HEHEHP. Hydrometallurgy, 137: 140-147. DOI: 10.1016/j.hydromet.2013.06.002

Luo, C., R. Wei, D. Guo, S. Zhang and S. Yan, 2013. Adsorption behavior of MnO_2 functionalized multi-walled carbon nanotubes for the removal of cadmium from aqueous solutions. Chem. Eng. J., 225: 406-415. DOI: 10.1016/j.cej.2013.03.128

Ma, Y., S.G. Wang, M. Fan, W.X. Gong and B.Y. Gao, 2009. Characteristics and defluoridation performance of granular activated carbons coated with manganese oxides. J. Hazardous Mater., 168: 1140-1146. DOI: 10.1016/j.jhazmat.2009.02.145

Mahmoud, M.A., 2015. Kinetics and thermodynamics of aluminum oxide nanopowder as adsorbent for Fe (III) from aqueous solution. Beni-Suef Univ. J. Basic Applied Sci., 4: 142-149. DOI: 10.1016/j.bjbas.2015.05.008

Mathur, R.B., J. Mittal, O.P. Bahl and N.K. Sandle, 1994. Characteristics of $KMnO_4$-modified PAN fibres-its influence on the resulting carbon fibres' properties. Carbon, 32: 71-77. DOI: 10.1016/0008-6223(94)90010-8

Mokhtari, S. and H. Faghihian, 2015. Modification of activated carbon by 2,6-diaminopyridine for separation of Hg^{2+} from aqueous solutions. J. Environ. Chem. Eng., 3: 1662-1668. DOI: 10.1016/j.jece.2015.06.002

Mopoung, S. and P. Amornsakchai, 2016. Microporous activated carbon fiber from pineapple leaf fiber by H_3PO_4 activation. Asian J. Sci. Res., 9: 24-33.

Mopoung, S., P. Amornsakchai and S. Somroop, 2016. Characterization of phosphoric acid modified activated carbon fiber from fiber waste of pineapple leaf fiber production processing. Carbon Sci. Technol., 8: 1-12.

Natkański, P., P. Kuśtrowski, A. Białas, Z. Piwowarska and M. Michalik, 2013. Thermal stability of montmorillonite polyacrylamide and polyacrylate nanocomposites and adsorption of Fe(III) ions. Applied Clay Sci., 75-76: 153-157. DOI: 10.1016/j.clay.2013.02.002

Ping, F., C. Chao-Ping and T. Zi-Jun, 2012. Experimental study on the oxidative absorption of Hg^0 by $KMnO_4$ solution. Chem. Eng. J., 198-199: 95-102. DOI: 10.1016/j.cej.2012.05.072

Sadeek, S.A., N.A. Negm, H.H.H. Hefni and M.M.A. Wahab, 2015. Metal adsorption by agricultural biosorbents: Adsorption isotherm, kinetic and biosorbents chemical structures. Int. J. Biol. Macromolecules, 81: 400-409. DOI: 10.1016/j.ijbiomac.2015.08.031

Shan, X., S. Zhu and W. Zhang, 2008. Effect of surface modification of activated carbon on its adsorption capacity for NH_3. J. China Univ. Min. Technol., 18: 261-265. DOI: 10.1016/S1006-1266(08)60055-3

Shrestha, S., G. Son, S.H. Lee and T.G. Lee, 2013. Isotherm and thermodynamic studies of Zn(II) adsorption on lignite and coconut shell-based activated carbon fiber. Chemosphere, 92: 1053-1061. DOI: 10.1016/j.chemosphere.2013.02.068

Song, W., Y. Li, X. Guo, J. Li and X. Huang *et al*., 2010. Selective surface modification of activated carbon for enhancing the catalytic performance in hydrogen peroxide production by hydroxylamine oxidation. J. Molecular Catalysis A: Chem., 328: 53-59. DOI: 10.1016/j.molcata.2010.05.022

Tian, J., M. Ernst, F. Cui and M. Jekel, 2013. $KMnO_4$ pre-oxidation combined with $FeCl_3$ coagulation for UF membrane fouling control. Desalination, 320: 40-48. DOI: 10.1016/j.desal.2013.04.017

Üçer, A., A. Uyanık, S. Çay and Y. Özkan, 2005. Immobilisation of tannic acid onto activated carbon to improve Fe(III) adsorption. Separat. Purificat. Technol., 44: 11-17. DOI: 10.1016/j.seppur.2004.11.011

Waller, G.H., S.Y. Lai, B.H. Rainwater and M. Liu, 2014. Hydrothermal synthesis of $LiMn_2O_4$ onto carbon fiber paper current collector for binder free lithium-ion battery positive electrodes. J. Power Sources, 251: 411-416. DOI: 10.1016/j.jpowsour.2013.11.081

Wang, Y., X. Wang, X. Wang, M. Liu and L. Yang *et al*., 2012. Adsorption of Pb(II) in aqueous solutions by bamboo charcoal modified with $KMnO_4$ via microwave irradiation. Colloids Surfaces A: Physicochemical Eng. Aspects, 414: 1-8. DOI: 10.1016/j.colsurfa.2012.08.007

Xie, X. and L. Gao, 2007. Characterization of a manganese dioxide/carbon nanotube composite fabricated using an in situ coating method. Carbon, 45: 2365-2373. DOI: 10.1016/j.carbon.2007.07.014

Yang, K., L. Yan, Y. Yang, S. Yu and R. Shan *et al*., 2014. Adsorptive removal of phosphate by Mg–Al and Zn–Al layered double hydroxides: Kinetics, isotherms and mechanisms. Separat. Purificat. Technol., 124: 36-42. DOI: 10.1016/j.seppur.2013.12.042

Yang, R., G. Liu, X. Xu, M. Li and J. Zhang *et al*., 2011. Surface texture, chemistry and adsorption properties of acid blue 9 of hemp (*Cannabis sativa* L.) bast-based activated carbon fibers prepared by phosphoric acid activation. Biomass Bioenergy, 35: 437-445. DOI: 10.1016/j.biombioe.2010.08.061

Zeid, N.A., G. Nakhla, S. Farooq and E. Osei-Twum, 1995. Activated carbon adsorption in oxidizing environments. Water Res., 29: 653-660. DOI: 10.1016/0043-1354(94)00158-4

Zhang, C., A. Song, P. Yuan, Q. Wang and P. Wang *et al*., 2016. Amorphous carbon shell on Si particles fabricated by carbonizing of polyphosphazene and enhanced performance as lithium ion battery anode. Mater. Lett., 171: 63-67. DOI: 10.1016/j.matlet.2016.02.034

Zhang, L., W. Wang, M. Shang, S. Sun and J. Xu, 2009. Bi_2WO_6@carbon/Fe_3O_4 microspheres: Preparation, growth mechanism and application in water treatment. J. Hazardous Mater., 172: 1193-1197. DOI: 10.1016/j.jhazmat.2009.07.123

Zhang, X.L., S. Yan, R.D. Tyagi and R.Y. Surampalli, 2013a. Odor control in lagoons. J. Environ. Manage., 124: 62-71. DOI: 10.1016/j.jenvman.2013.03.022

Zhang, Y., Y. Wang and L. Zhou, 2013b. Influence of excess $KMnO_4$ on the adsorption of powdered activated carbon. Chem. Eng. J., 226: 279-285. DOI: 10.1016/j.cej.2013.03.063

Zhang, Y., C. Zhang, G. Huang, B. Xing and Y. Duan, 2015. Synthesis and capacitive properties of manganese oxide nanoparticles dispersed on hierarchical porous carbons. Electrochimica Acta, 166: 107-116. DOI: 10.1016/j.electacta.2015.03.073

Zhao, X., J. Chen, F. Chen, X. Wang and Q. Zhu *et al*., 2013. Surface characterization of corn stalk superfine powder studied by FTIR and XRD. Colloids Surfaces B: Biointerfaces, 104: 207-212. DOI: 10.1016/j.colsurfb.2012.12.003